Journal of Engineering and Sustainable Development
Vol. 30, No. 03, May 2026
https://jeasd.uomustansiriyah.edu.iq/index.php/jeasd
ISSN 2520-0917
Research Article
https://doi.org/10.31272/jeasd.2275

Behavior of Fibrous High-Strength Glass Fiber Reinforced Polymer Reinforced Concrete Deep Beams

Eklas Hatto Hashim*, Hassan Falah Hassan

Civil Engineering Department, College of Engineering, Mustansiriyah University, Baghdad, Iraq

*Email: eaph003@uomustansiriyah.edu.iq

Article Info

Received 19/10/2024
Revised 02/04/2026
Accepted 14/04/2026

Abstract

Deep beams are an important element in infrastructure and offshore structures. This paper investigates the shear capacity of glass fiber reinforced polymer GFRP reinforced high-strength fibrous concrete deep beam. (12) supported concrete deep beams with (GFRP) reinforcement have a cross-section of 150×340 mm under a one-point load and have been tested to fail. The test variables were the vertical web reinforcement ratio (0, 0.0025, 0.004, and 0.0053) and steel fiber volume fraction (0, 0.5, and 1%). All beams have a length of 1020mm, an effective span of 620mm, and an effective span-to-depth ratio of 1.02. The longitudinal reinforcement is 3D16 mm at the bottom and 2D6mm at the top. The test results analysis shows that the increase of vertical web reinforcement ratio from (0 to 0.0053) increases the failure load by (7.88 and 15.44) and decreases mid span deflection by (15.52 and 22.95) for fiber volume fraction (0 and 1%), respectively. Also, when the vertical web reinforcement ratio increases from (0 to 0.0053), the flexural crack increases by (20.02 and 29.50%) and the diagonal crack load by (38.5 and 51.15%) for fiber volume fraction (0 and 1%), respectively.

Keywords: Deep beams, Glass fiber reinforced polymer, Shear prediction equation, Steel fiber ratio, Vertical web reinforcement ratio.

1. Introduction

Deep beams are members with a small span relative to their depth. ACI 318-19 code [1] defines a deep beam as a member that the load applied on one face and supported on the inverse face strut compression element can create along the path between the load and the support, and that achieves (a clear span ≤ 4 times overall member depth, or shear span a ≤ 2 times overall member depth) [1]. CSA A-23.3-04 [2] defines a deep beam as a deep flexural member with a clear span to overall depth < 2. The strain distribution over the cross-section of a deep beam cannot be regarded as linear; there will be noticeable shear deformation in comparison to pure flexure. Typically, shear rather than flexure governs the strength of deep beams.

The concrete contribution to shear capacity is assumed to arise from resistance across the concrete compressive zone, dowel action, and aggregate interlock [1], [3]. Numerous steel-reinforced concrete structures, such as marine structures, structures exposed to high humidity, parking lots, and bridges, can over time result in substantial damage and the need for expensive rehabilitation due to corrosion of steel reinforcements. It is becoming more common to specify members internally reinforced with fiber-reinforced polymer (FRP) to reduce corrosion-induced damage in concrete construction.

A fiber-reinforced polymer (FRP) bar-composite material, composed mostly of longitudinal unidirectional fibers bound and molded with a rigid polymer resin, is fashioned into a long, slender structural shape suitable for interior reinforcement of concrete. Glass fiber-reinforced polymer (GFRP) bars are linear elastic until failure and do not yield. Additionally, GFRP bars exhibit high tensile strength in the reinforcing fiber direction, which affects shear strength, bond performance, and dowel action [4].

Research studies on FRP-RC deep beams with web reinforcement often use GFRP, which is readily available and cheaper [5]-[7]. The lack of ductility in structural concrete components reinforced with FRP bars should be considered in design, and the member should have a greater reserve of strength. According to test data, FRP-reinforced deep beams behave differently from steel-reinforced deep beams in terms of shear strength, deformation, and fracture width [8].

High-strength concrete can increase the cracked section's stiffness and better leverage FRP bars' high-strength properties. Still, because it is more brittle than normal-strength concrete, it

can also reduce the overall deformability of flexural strength [4].

FOR THE FRP RC deep beam, the increasing compressive strength increases shear capacity for the same longitudinal and web reinforcement ratio [5], [9]. The post cracking stiffness of the beam is not affected or little affected by the concrete strength [7],[10],[11]. The addition of steel fiber to the concrete mixture can significantly increase the concrete's contribution to shear strength, reducing deformations and enhancing cracking behavior, and altering the shear-to-flexural failure mode in some beams [12]-[13].

The use of a steel fiber layer in the tie zone led to soft deflection behavior, with failure more ductile rather than brittle or sudden. Also, the effect of steel fiber is more than that of basalt fiber because of the higher elasticity of steel [14]. Basalt fiber-reinforced polymer (BFRP) short beams exhibit significant improvements in overall stiffness, toughness, and ultimate shear strength due to the presence of basalt microfibers and synthetic fibers. The addition of basalt microfibers reduces the beams' mid-span deflection and increases overall stiffness [11].

In this paper, we study the behavior of a GFRP RC deep beam with vertical web reinforcement and steel fiber reinforcement.

The efficient use of FRP reinforcement, in general, and fiber reinforcement, in particular, in deep members has been limited due to a lack of understanding of their behavior. Due in part to the lack of experimental data, the ACI code does not provide design guidelines for deep FRP-reinforced concrete beams. This paper presents the findings of an experimental investigation of concrete deep beams internally reinforced with GFRP.

2. Methods and Materials

2.1. Test Summary

Twelve concrete deep beams with GFRP reinforcement were built and tested to failure in high-strength fibrous concrete in the Structural Laboratory of Engineering College at Mustansiriyah University. The test specimen dimensions: height, width, and length ($h \times bw \times l$) are ($340 \times 150 \times 1020$) mm. The specimens were designed with adequate longitudinal tension reinforcement ($\rho = 1.30\%$) for all specimens to ensure shear failure. The loading plate and support plate were ($95 \times 150 \times 25$) mm and ($95 \times 150 \times 15$) mm respectively. The adopted parameters include vertical web reinforcement (ρv) and fiber volume fraction (Vf). The shear span to effective depth ratio was ($a/d = 1.02$) for all specimens.

Strain gauges of 5 mm and 60 mm were used to measure strain in the reinforcement and concrete, respectively. The naming of specimens, for example, is as follows:

F0V25

Fiber ratio%, Vertical web reinforcement ratio per 10000

2.2. Experimental Material

The current study uses Ordinary Portland cement (Type I), Fine aggregate, crushed gravel with a maximum size of 10mm, silica fume, superplasticizer, end-hook steel fiber (30mm length, 0.375 mm diameter), and water. The water/cement ratio was 0.26, and wood moldings of type plywood (15mm) thickness were used to cast the beam. The mechanical properties of the GFRP bar used are shown in Table 1. The content weight per cubic meter is shown in Table 2.

The mechanical properties of the concrete specimens are shown in Table 3; these properties are approximately the same age as the deep beams tested.

Table 1. The properties of the GFRP bar.

Diameter mm	Nominal area mm²	f_u MPa	E_f GPa.	Weight g/m
6	29	896		77.4
8	50	850	46	121.44
16	197.9	724		427.1

Where $f_u$the ultimate tensile strength of the GFRP bar, Ef, is the modulus of elasticity of the GFRP bar.

Where f'_c is concrete compressive strength, f_t is the splitting tensile strength of concrete, f_r is the modulus of rupture of concrete, E_c is the modulus of elasticity of concrete.

Table 2. Weight of contents per cubic meter.

Mix Type	Cement kg	Sand kg	Gravel kg	Silica fume kg	Super Plasticizer liter	Water liter	Fiber kg
F0							0
F0.5	650	900	500	105	20.8	169	39.375
F1							78.75

Table 3. The properties of specimens.

Specimen	h mm	b_w mm	a/d	d mm	ρ %	Fiber volume %	ρ_v %	f'_c Ave. MPa.	f_t Ave. MPa.	f_r Ave. MPa.	E_c Ave. MPa.
F0V0	340	150	1.02	304	1.30	0	0	52.08	3.47	4.17	31.46
F0V25							0.25				
F0V40							0.40				
F0V53							0.53				
F0.5V0						0.5	0	61.12	6.4	6.92	32
F0.5V25							0.25				
F0.5V40							0.40				
F0.5V53							0.53				
F1V0						1	0	66.6	8.47	8.63	33.03
F1V25							0.25				
F1V40							0.40				
F1V53							0.53				

2.3. Specimen Details

Fig. 1 shows the details of the beam's geometry and reinforcement. The details are repeated for three fiber volume fractions. The symbols BC and DC indicate the strain gauges at the bottom and diagonal positions on the beam's concrete surface, respectively. In contrast, symbols BG and VG indicate the strain gauge at the bottom and the stirrup reinforcement of the beam, respectively.

2.4. Instrument and Test Procedure

A universal testing machine of the Engineering College's Structural Laboratory at Mustansiriyah University was used in testing. Fig. 2 shows the test loading device. The load increment rate was about 5 kN /sec. An LVDT was used to measure the deflection at the center of the bottom beam. An electrical system (a data logger) was used to record data. Also, two cameras were used to record the stages of beam failure.

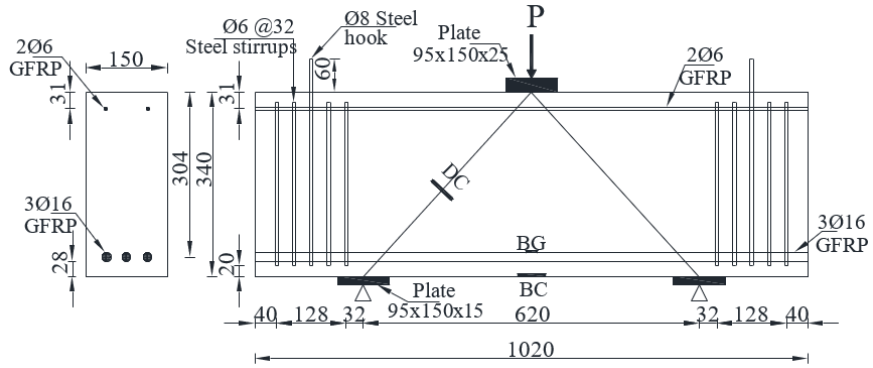

(a) F0V0, F0.5V0, F1V0.

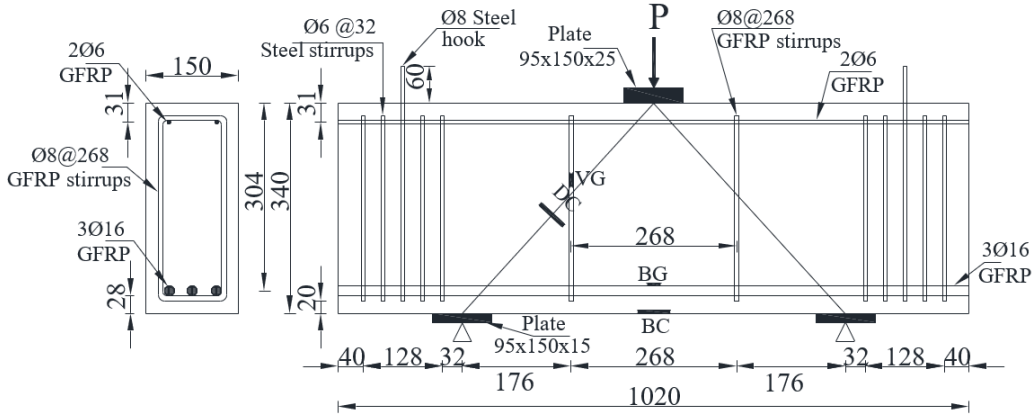

(b) F0V25, F0.5V25, F1V25.

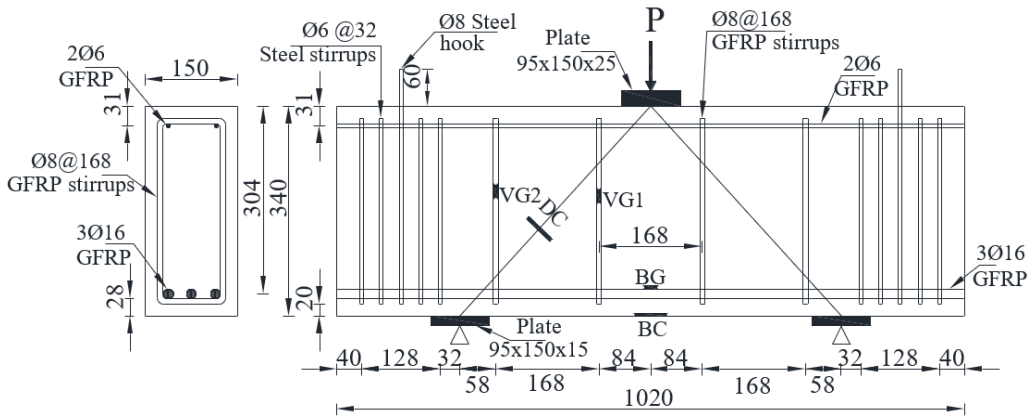

(c) F0V40, F0.5V40, F1V40.

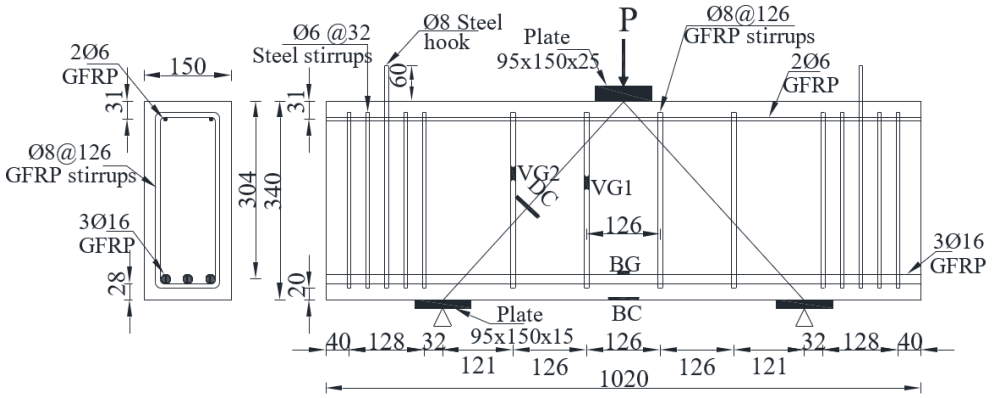

(d) F0V53, F0.5V53, F1V53.

Figure 1. The details of the beam's geometry and reinforcement.

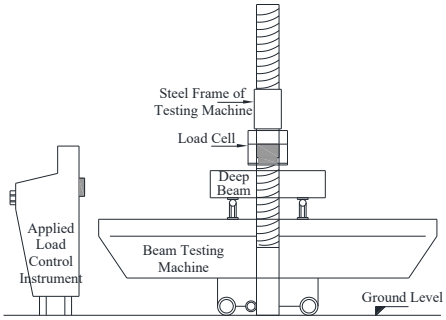

(a) Schematic diagram of the loading device.

(b) LVDT instrument.

(c) Loading device and test accessories.

Figure 2. Test Loading.

3. Results and Discussions

The effect of the specimen's parameters on the test result can be summarized as follows:

3.1 Failure Load and Strains

The specimens will be divided into three groups according to the fiber volume fraction used: 0%, 0.5%, and 1%. Each group has a different vertical web reinforcement ratio (0, 0.0025, 0.004, and 0.0053).

Despite the deep beam's specimen parameters varying in this study, loading stages can be divided into three stages of failure progression. The stages are first flexural crack, first diagonal crack, and failure. The load and the associated effects for specification of the deep beam are specimens for the first flexural crack, first diagonal crack, and maximum failure load, deflection at mid span (*Δ*This study discusses the tensile reinforcement strain, bottom concrete strain, and diagonal concrete strain.

As listed in Table 4, when vertical web reinforcement increases from (0, to 0.0025, 0.0040 and 0.0053), the failure load of the specimens increases by (2.51, 4.45 and 7.88%), (4.34, 7.64 and 11.91%), and (2.03, 7.76, 15.44%) for the fiber volume fraction (0, 0.5, and 1%) respectively. It can be noted that the failure load ratio increases as the fiber volume fraction increases for the same vertical web reinforcement. Fig. 3 shows the parameter's effect on max load.

3.2 Mid Span Deflection (Δ)

Returning also to Table 4, when vertical web reinforcement increases from (0, to 0.0025, 0.0040 and 0.0053), the mid span deflection at minimum load reported (0 vertical web reinforcement specimen) for group fiber fraction volume (0, 0.5 and 1%) were decrease by (13.75, 23.39 and 32.89%), (19.12, 31.43 and 38.52%) and (19.03, 31.20 and 44.73%) respectively.

Despite the type of failure that contributes to deflection, the average mid-span deflection at max load decreases with increasing vertical web reinforcement ratio, even as the failure load increases, as shown in Fig. 4.

Table 4. Max load test result of specimens.

Specimen	P_{max} kN	Δ at P_{max} mm	Bottom concrete strain at P_{max}	Diagonal concrete strain at P_{max}	Tensile reinforcement strain at P_{max}	Failure type
F0V0	558.11	6.65	0.00018	0.00021	0.00520	Strut crushing
F0V25	572.11	5.90	0.00014	0.00009	0.00471	Strut crushing
F0V40	582.96	5.72	0.00020	0.00033	0.00410	Shear compression
F0V53	602.08	5.62	0.00021	0.00012	0.00390	Shear compression
F0.5V0	579.96	7.25	0.00014	0.00014	0.00573	Strut crushing
F0.5V25	605.13	6.21	0.00022	0.00014	0.00510	Shear compression
F0.5V40	624.26	5.81	0.00016	0.00034	0.00450	Shear compression
F0.5V53	649.03	5.67	0.00018	0.00015	0.00421	Shear compression
F1V0	609.16	8.10	0.00012	0.00032	0.00651	Strut crushing
F1V25	621.53	7.32	0.00013	0.00015	0.00580	Strut crushing
F1V40	656.41	7.11	0.00017	0.00034	0.00500	Shear compression
F1V53	703.21	6.24	0.00029	0.00015	0.00482	Shear compression

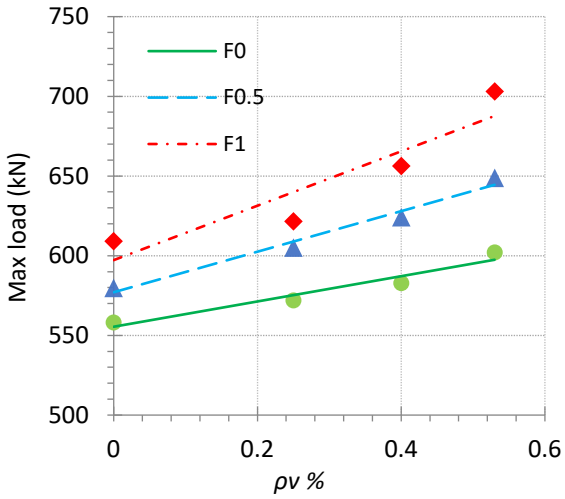

(a) Effect of steel fiber content on max load.

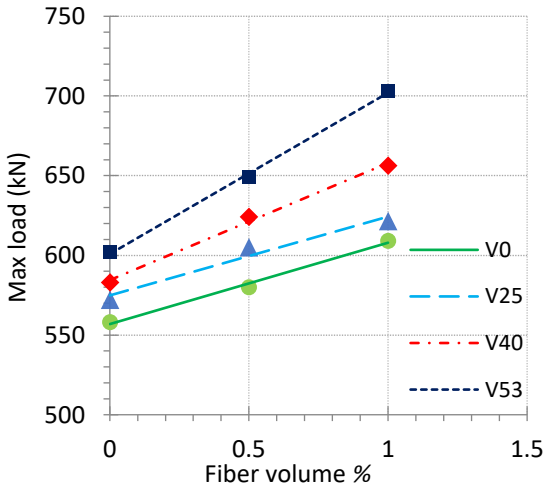

(b) Effect of vertical web reinforcement on max load.

Figure 3. Parameters' effect on max load.

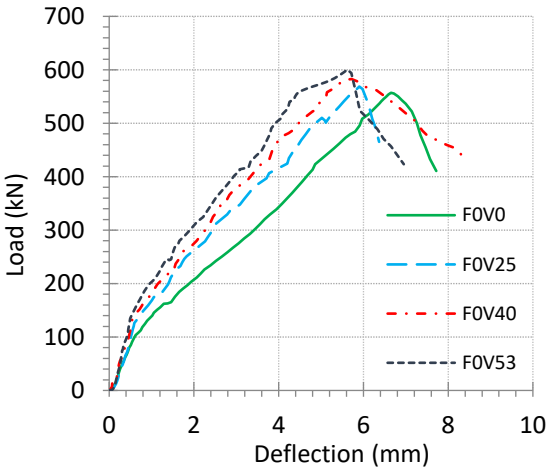

(a) Effect of vertical web reinforcement ratio on deflection for 0% steel fiber content.

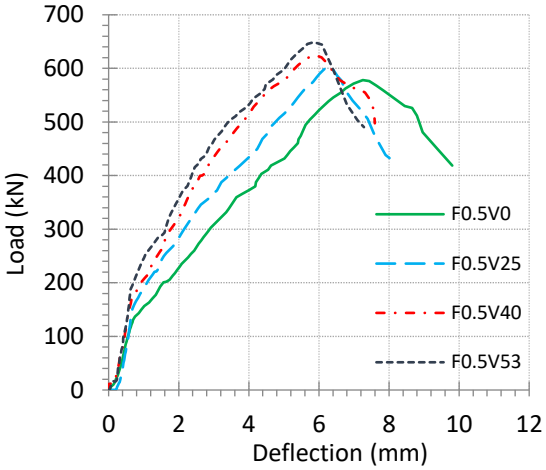

(b) Effect of vertical web reinforcement ratio on deflection for 0.5% steel fiber content.

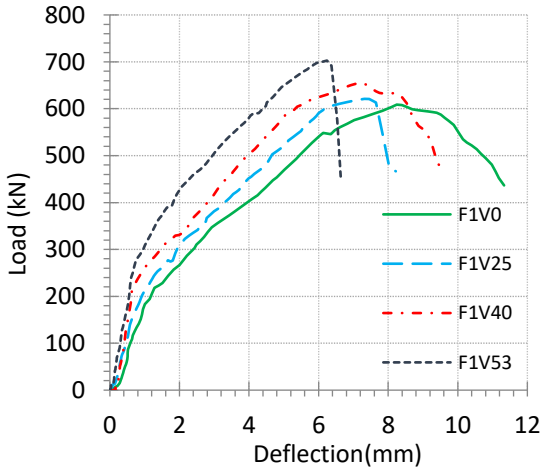

(c) Effect of vertical web reinforcement ratio on deflection for 1% steel fiber content.

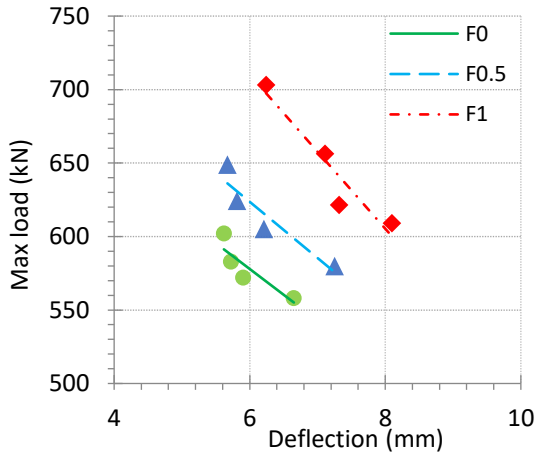

(d) Relation between max load and deflection for different steel fiber content.

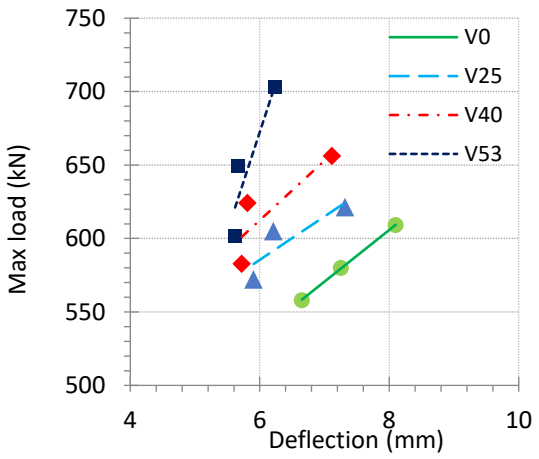

(e) Relation between max load and deflection for different web reinforcement ratios.

Figure 4. Parameters' effect on mid-span deflection at max load.

3.3 Failure Modes and Crack Patterns

Two types of failure (strut crushing and shear compression failure) were observed. Most of the beams, for all fiber volume fraction, with vertical web reinforcement ($\rho_v = 0, 0.0025$) had a strut crushing failure, while beams with vertical web reinforcement ($\rho_v = 0.004, 0.0053$) had shear-compression failure, as previously given in Table 4.

The first crack was mostly vertical for all specimens and formed at the bottom of the beam under the loading point within the range given in Table 5. For a beam without a volume fraction of fiber, as the load increased, one or two new flexural cracks formed, and additional flexural cracks formed near the first. For most specimens, most of the flexural cracks stop over a few distances, except for specimens (F0V40, F1V40, F0V53, and F1V53), the crack continues with increasing load till the failure, where it reaches the loading point as shown in Fig.5.

More cracks were present in the beams with low vertical web reinforcement ($\rho_v = 0, 0.0025$) than in beams with more vertical web reinforcement ($\rho_v = 0.004, 0.0053$). Flexure cracks were very thin and were not affected by fiber content due to the high tension reinforcement ratio.

Shear failure occurs when the stress exceeds the concrete's allowable shear stress, and an inclined crack forms. The presence of vertical web reinforcement or fiber delays or limits the development of the cracks.

The initial diagonal crack in the specimen forms at the load given in Table 6. The diagonal crack formed at the inside edge of the support plate in the direction of the inside of the loading plate. For beams without fiber volume fraction, as the load increased, diagonal cracks multiplied, extended rapidly, and those already present expanded or stretched. For beams with fiber volume fraction, as the load increases, no more diagonal cracks; a little slower, extended, and expanded.

The most important feature of cracks in beams with fiber volume fraction is that they are not sharp, because the two crack faces are bridged by fibers and resist tensile forces, thereby increasing the load capacity to failure.

Some loading point regions gradually deteriorated through unloading for beams with web reinforcement, especially ($\rho_v = 0, 0.0025$).

(a) strut crushing failure.

(b) strut crushing failure.

(c) shear compression failure.

(d) shear compression failure.

Figure 5. Specimen picture after unloading.

3.4 Tensile Reinforcement Strain

As previously mentioned in Table 4, when vertical web reinforcement increases from (0, to 0.0025, 0.0040 and 0.0053), the tensile reinforcement strain at minimum load reported (0 vertical web reinforcement specimen) for group fiber fraction volume (0, 0.5 and 1%) were decrease by (11.32, 23.73 and 34.15%), (16.26, 30.96 and 41.21%) and (16.50, 34.86 and 44.52%) respectively.

The average tensile reinforcement strain at the maximum load decreases with increasing vertical web reinforcement ratio for the same fiber volume fraction, despite the increase in failure load, as shown in Fig. 6.

3.5 Flexural Crack Load $(PF)_{cr}$

Visual inspection is often used to determine which load causes the first flexural crack. When using the concrete strain gauge at the expected flexural crack position, it helps accurately determine the crack load. It is noted that a change in the strain

gauge data is observed, which is due to the occurrence of a crack.

The flexural crack may stop at a specific load or continue until failure. This is evident from the relationship between the load and the bottom concrete strain, as shown in Fig. 7. This is due to the redistribution of stresses after the formation of a diagonal crack or other cracks.

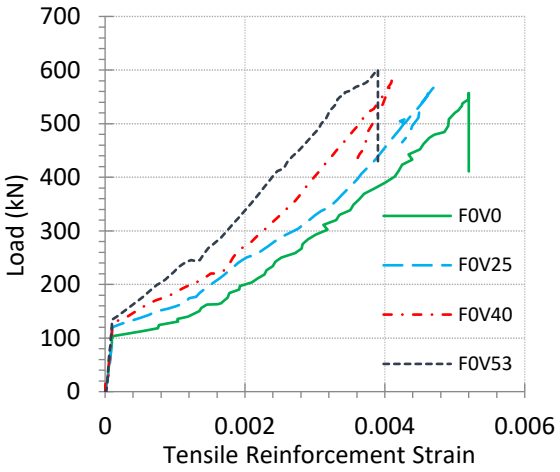

(a) Effect of vertical web reinforcement ratio on tensile reinforcement strain for 0% steel fiber content.

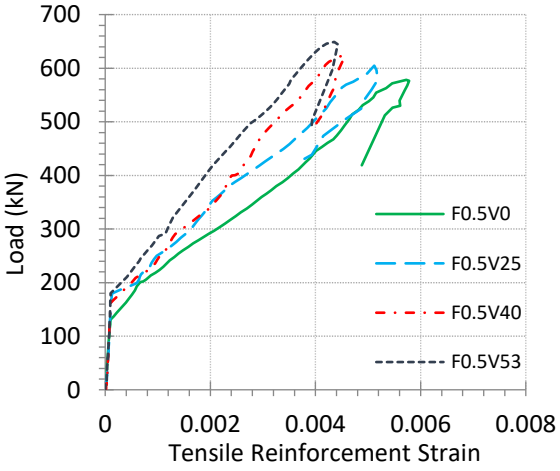

(b) Effect of vertical web reinforcement ratio on tensile reinforcement strain for 0.5% steel fiber content.

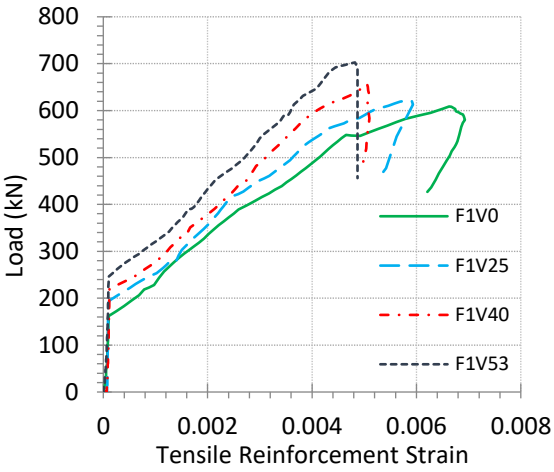

(c) Effect of vertical web reinforcement ratio on tensile reinforcement strain for 1% steel fiber content.

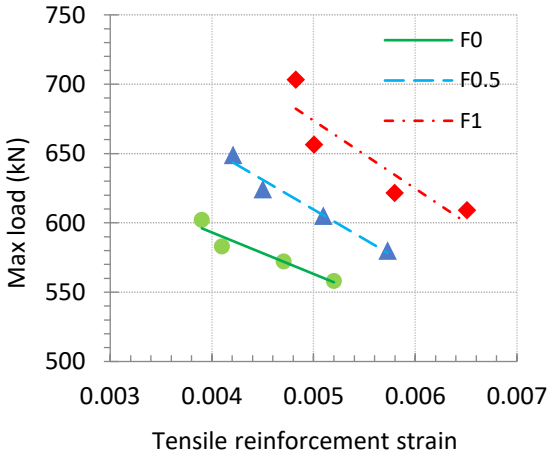

(d) Relation between max load and tensile reinforcement strain for different steel fiber content.

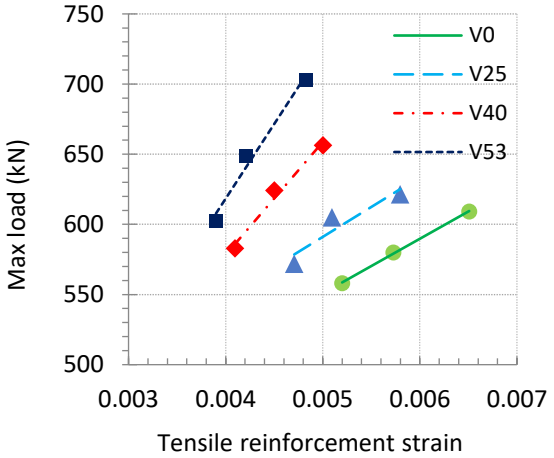

(e) Relation between max load and tensile reinforcement strain for different web reinforcement ratios.

Figure 6. Parameters' effect on tensile reinforcement strain at max load.

Table 5 show the flexural crack load for the specimens, when vertical web reinforcement increases from (0, to 0.0025, 0.0040 and 0.0053), the flexure crack load percent of max load of the specimens was increased by (12.98, 19.48 and 20.02%) ratio, (6.31, 15.29 and 23.41%) ratio and (16.43, 25.24, 29.50%) ratio for the fiber volume fraction (0, 0.5, and 1%) respectively.

On the other hand, when the fiber volume fraction increases from (0 to 0.5, and 1%), the flexure crack load percent of max load of the specimens was increases by (20.35,13.25, 16.14 and 23.75%) and (43.46, 47.84, 50.38 and 54.80%) for vertical web reinforcement increases from (0, to 0.0025, 0.0040 and 0.0053) respectively.

It can be observed that the flexural crack load increases by a larger percentage when the fiber volume fraction is increased than when the vertical web reinforcement ratio is increased, as shown in Fig. 7.

3.6 Diagonal Crack Load $(PD)_{cr}$)

The concrete strain gauge was placed on one side perpendicular to the path between the support and the applied load point. If the strain gauge is on the same side as the diagonal crack that occurred, in a similar way that the flexural crack load is determined, the diagonal crack load can be determined. Otherwise, determine the diagonal crack load by looking.

It is known as the compression region and tension region along the cross-section of the beam, which change with increased loading; the diagonal strain gauge records compression strain at the beginning of load application, then turns into tension. The amount of compression strain is very small for most specimens and higher for specimens F0.5V40, F0.5V53, F1V25, F1V40, and F1V53, which have high failure loads; it will be neglected relative to the diagonal strain with load.

Table 5. Flexure crack test result of specimens.

Specimen	$P_{F)cr}$ Flexure crack load kN	Δ at Flexure crack load mm	Bottom concrete strain at Flexure crack load	Tensile reinforcement strain at the flexure crack load	P_{max} kN	$P_{F)cr}$ /P_{max} %
F0V0	106.54	0.62	0.00011	0.00010	558.11	19.09
F0V25	123.39	0.58	0.00012	0.00010	572.11	21.57
F0V40	132.96	0.54	0.00011	0.00010	582.96	22.81
F0V53	137.94	0.50	0.00010	0.00010	602.08	22.91
F0.5V0	133.24	0.70	0.00012	0.00010	579.96	22.97
F0.5V25	147.80	0.66	0.00012	0.00010	605.13	24.42
F0.5V40	165.36	0.63	0.00012	0.00010	624.26	26.49
F0.5V53	184.02	0.61	0.00013	0.00010	649.03	28.35
F1V0	166.82	0.92	0.00012	0.00010	609.16	27.39
F1V25	198.18	0.88	0.00013	0.00012	621.53	31.89
F1V40	225.14	0.68	0.00012	0.00012	656.41	34.30
F1V53	249.39	0.64	0.00012	0.00010	703.21	35.46

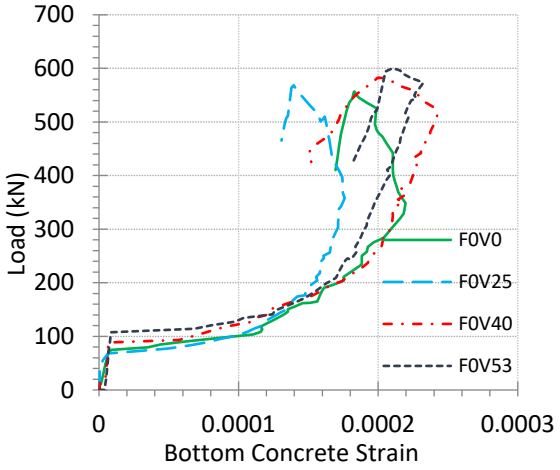

(a) Effect of vertical web reinforcement on bottom concrete strain for 0% steel fiber content.

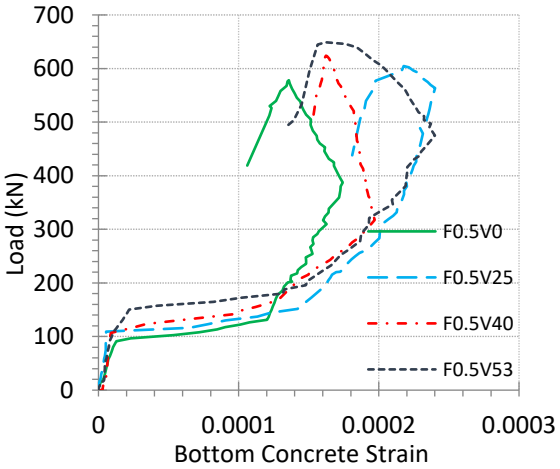

(b) Effect of vertical web reinforcement on bottom concrete strain for 0.5% steel fiber content.

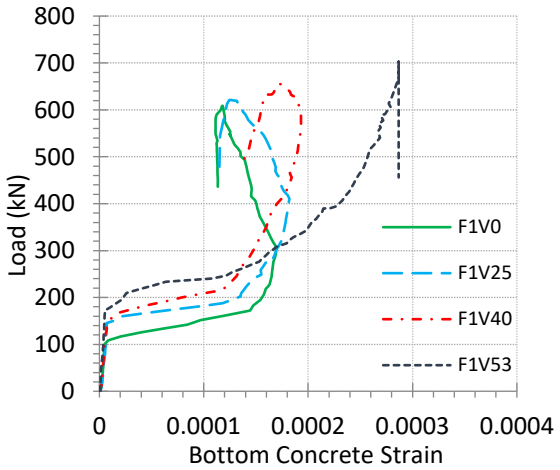

(c) Effect of vertical web reinforcement on bottom concrete strain for 1% steel fiber content.

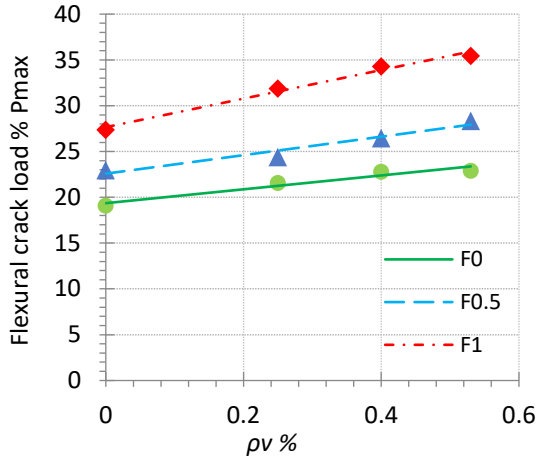

(d) Relation between flexural crack load % *Pmax* and vertical web reinforcement for different steel fiber content.

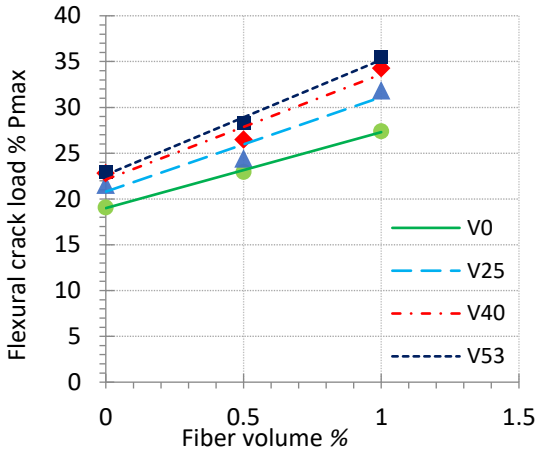

(e) Relation between flexural crack load % *Pmax* and steel fiber content for different vertical web reinforcement.

Figure 7. Parameters' effect on flexural crack load.

Table 6 show the diagonal crack load for the specimens, when vertical web reinforcement increases from (0, to 0.0025, 0.0040 and 0.0053), the diagonal crack load percentage of max load of the specimens was increases by (5.02, 28.96 and 38.47%) ratio, (4.28, 19.26 and 27.48%) ratio and (21.87, 37.60, 51.15%) ratio for the fiber volume fraction (0, 0.5, and 1%) respectively. The diagonal crack load percentage at maximum load increases with increasing fiber volume fraction and vertical web reinforcement ratio, as shown in Fig. 8.

3.7. Ductility Index

The ductility index or deformability factor of a structure is a measurement of a material's capacity to withstand significant deformation and absorb energy before failing.

Table 6. Diagonal crack test result of specimens.

Specimen	$P_{D)cr}$ Diagonal crack load. kN	Δ at the diagonal crack load mm	Bottom concrete strain at the diagonal crack load	Diagonal concrete strain at Diagonal crack load	Tensile reinforcement strain at the diagonal crack load	P_{max} kN	$P_{D)cr}/P_{max}$ %
F0V0	165.56	1.29	0.00015	0.00011	0.00145	558.11	29.66
F0V25	178.23	1.05	0.00014	0.00009	0.00120	572.11	31.15
F0V40	223.00	1.42	0.00018	0.00011	0.00151	582.96	38.25
F0V53	247.31	1.37	0.00018	0.00009	0.00123	602.08	41.08
F0.5V0	204.42	1.56	0.00014	0.00011	0.00067	579.96	35.25
F0.5V25	222.43	1.31	0.00017	0.00011	0.00073	605.13	36.76
F0.5V40	262.42	1.47	0.00017	0.00011	0.00109	624.26	42.04
F0.5V53	291.64	1.43	0.00019	0.00012	0.00102	649.03	44.94
F1V0	225.03	1.28	0.00016	0.00012	0.00078	609.16	36.94
F1V25	279.81	1.67	0.00016	0.00012	0.00126	621.53	45.02
F1V40	333.66	1.88	0.00015	0.00012	0.00147	656.41	50.83
F1V53	392.64	1.64	0.00021	0.00012	0.00163	703.21	55.84

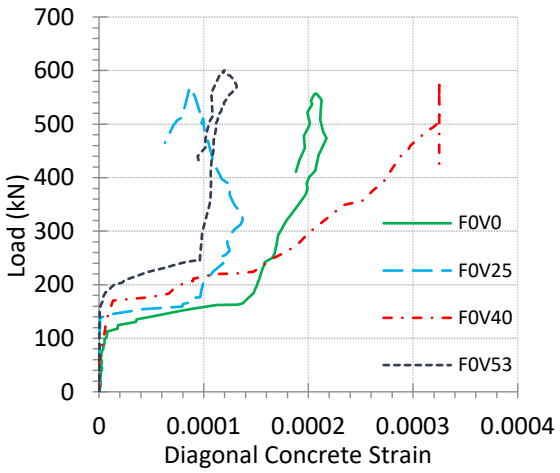

(a) Effect of vertical web reinforcement on diagonal concrete strain for 0% steel fiber content.

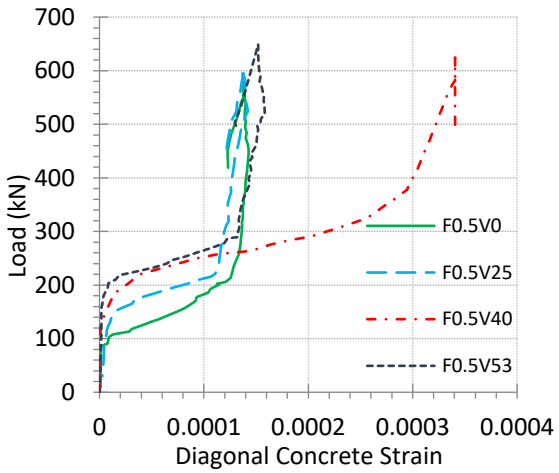

(b) Effect of vertical web reinforcement on diagonal concrete strain for 0.5% steel fiber content.

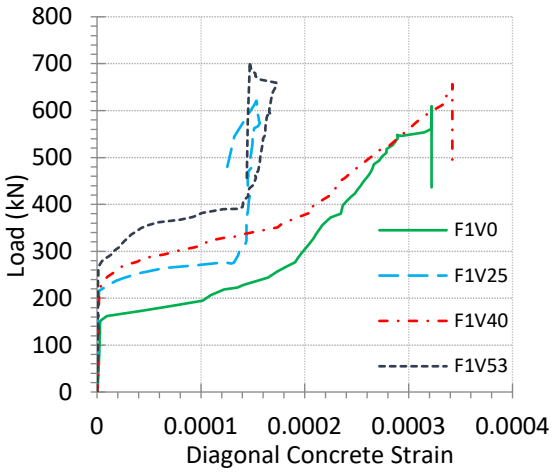

(c) Effect of vertical web reinforcement on diagonal concrete strain for 1% steel fiber content.

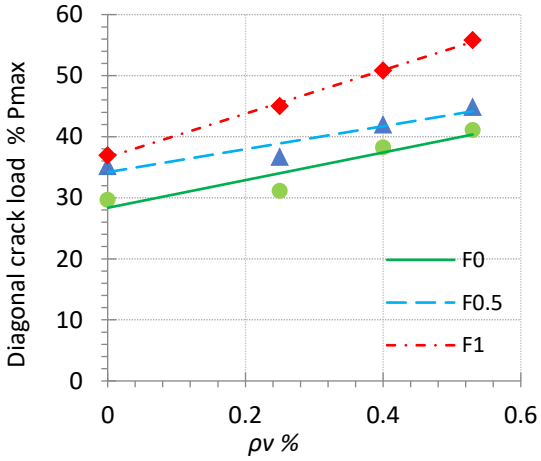

(d) Relation between diagonal crack load % *Pmax* and web reinforcement ratio for different steel fiber content.

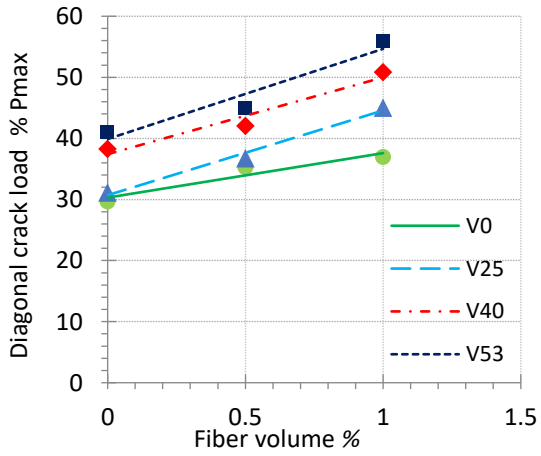

(e) Relation between diagonal crack load % *Pmax* and steel fiber content for different web reinforcement ratios.

Figure 8. Parameters' effect on the diagonal crack load.

The ability of a structure to undergo considerable deformations without sudden, catastrophic failure makes ductility an important attribute in structural engineering, as it can provide warning signs and allow occupants time to flee in the event of excessive loading. The true ductility index for a structure must frequently be determined by experimental testing and analysis.

ACI 440.1R-15 [15] defines the deformability factor "Ratio of energy absorption (area under the moment curvature curve) at ultimate strength of the section to the energy absorption at service level".

Due to the lack of a yield point in glass-fiber-reinforced (GFR) concrete, conventional definitions of ductility do not apply to assessing the ductility of GFR concrete beams [16]. Jaejer et al. [17] emphasized that, when discussing FRP reinforcement, the concept of deformability takes precedence over ductility.

Spadea et al. [18] proposed the energy ductility (μ_{en}) to be expanded as follows

$$\mu_{en} = \frac{E_{tot}}{E_{0.75pu}} \quad (1)$$

Where E_{tot} (total energy) is the area under the load deflection curve up to the ultimate load and $E_{0.75pu}$Is the area under the load-deflection curve up to 0.75 the ultimate load?

Based on the corresponding deformation at the ultimate and the uncracked section, for beams prestressed by FRP tendons, Abdelrahman et al. [19] suggest a ductility model ($\mu\Delta$) as follow:

$$\mu\Delta = \Delta 2 \Delta 1 \quad (2)$$

Where Δ1 and Δ2 are the deflections as shown in Fig. 9.

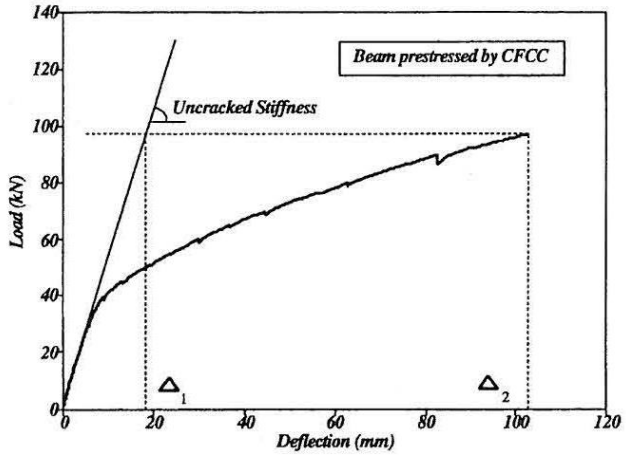

Figure 9. Proposed procedure for evaluating the member ductility of concrete beams prestressed with FRP [19].

The load-deflection curve for the deep beam in the current study contains two parts: the uncracked beam's performance represents the initial segment of the curve up to the crack, and the linear part extends approximately to failure. The most appropriate method for determining the ductility index in this study is that of Spadea et al. [18] and Abdelrahman et al. [19].

The results of determining the ductility index using Spadea et al. [18] and Abdelrahman et al. vary greatly, as shown in Table 7.

Generally, in both Spadea et al. [18] and Abdelrahman et al. [19], the ductility index is affected by the web reinforcement parameter and the fiber volume fraction, as shown in Figs. 10 and 11.

By using Spadea et al. method [15], when the fiber volume fraction increases from (0 to 0.5% and 1%), the ductility index was increased by (4.49, 5.73, 19.30 and 16.32%) and (30.19, 35.66, 27.99 and 28.05%) for vertical web reinforcement increases from (0, to 0.0025, 0.0040 and 0.0053) respectively.

On the other hand, when vertical web reinforcement increases from (0, to 0.0025, 0.0040 and 0.0053), the ductility index was increase by (0.64, 12.27 and 17.84%) ratio, (1.84, 28.18 and 31.18%) ratio and (4.87, 10.37, 15.89%) ratio for the fiber volume fraction (0, 0.5, and 1%) respectively.

By using Abdelrahman et al. method, when the fiber volume fraction increases from (0 to 0.5% and 1%), the ductility index was increased by (22.83, 3.05, -1.23, and 6.18%) and (30.49, 16.27, 36.41 and 34.24%) for vertical web reinforcement increases from (0, to 0.0025, 0.0040 and 0.0053) respectively.

On the other hand, when vertical web reinforcement increases from (0, to 0.0025, 0.0040 and 0.0053), the ductility index was increase by (18.85, 31.01 and 33.72%) ratio, (-0.29, 5.34 and 15.59%) ratio and (5.90, 36.96 and 37.56%) ratio for the fiber volume fraction (0, 0.5, and 1%) respectively.

It can be noted that the web reinforcement increases ductility to a greater extent than increasing fiber volume fraction.

Table 7. The ductility of specimens.

Specimen	P_{max} kN	Deflection Δ at P_{max} mm	Spadea et al. [18] μ_E	Abdelrahman et al. [19] μ_Δ
F0V0	558.11	6.65	1.80	1.90
F0V25	572.11	5.90	1.81	2.26
F0V40	582.96	5.72	2.02	2.50
F0V53	602.08	5.62	2.12	2.55
F0.5V0	579.96	7.25	1.88	2.34
F0.5V25	605.13	6.21	1.92	2.33
F0.5V40	624.26	5.81	2.41	2.46
F0.5V53	649.03	5.67	2.47	2.70
F1V0	609.16	8.10	2.35	2.49
F1V25	621.53	7.32	2.46	2.63
F1V40	656.41	7.11	2.59	3.40
F1V53	703.21	6.24	2.72	3.42

According to CSA A23.3-19 [2], [20], the modification factors of ductility-related force of moment resisting frame are (4.0), which is also recommended by CSA S806-12. The deep beam is not considered a moment-resisting frame; there is no ductility index specifically for deep beams.

3.8 Shear Capacity Prediction Methods and Test Results

There is a lot of research on methods of predicting the shear capacity of FRP RC deep beams, especially those making improvements to the STM method [8], [21].

Four methods used to predict the shear capacity of FRP reinforced deep beam will be used to compare with the test result; these methods of prediction are as follows:

3.8.1 Shear Concrete Capacity V_c ACI 440.11- 22 [4]

Shear strength prediction of FRP reinforced according to ACI 440.1R-15 [13], for a slender beam, is similar to that of a steel-reinforced beam, considering the variation between the steel and FRP's elasticity modulus. In ACI 440.11-22 [4], the size effect component is included for calculating shear capacity.

$$V_c = 0.42\sqrt{f_c'}\, b_w \lambda_s k d \quad (3)$$

$$k = \sqrt{2\rho_f n_f + (\rho_f n_f)^2} - \rho_f n_f \quad (4)$$

$$n_f = \frac{E_f}{E_c} \quad (5)$$

$$\lambda_s = \sqrt{\frac{2}{1+0.004*d}} \geq 1.0 \quad (6)$$

Where ρ_f is the longitudinal reinforcement ratio, Ec is the modulus of elasticity of concrete. λ_s size effect modification factor.

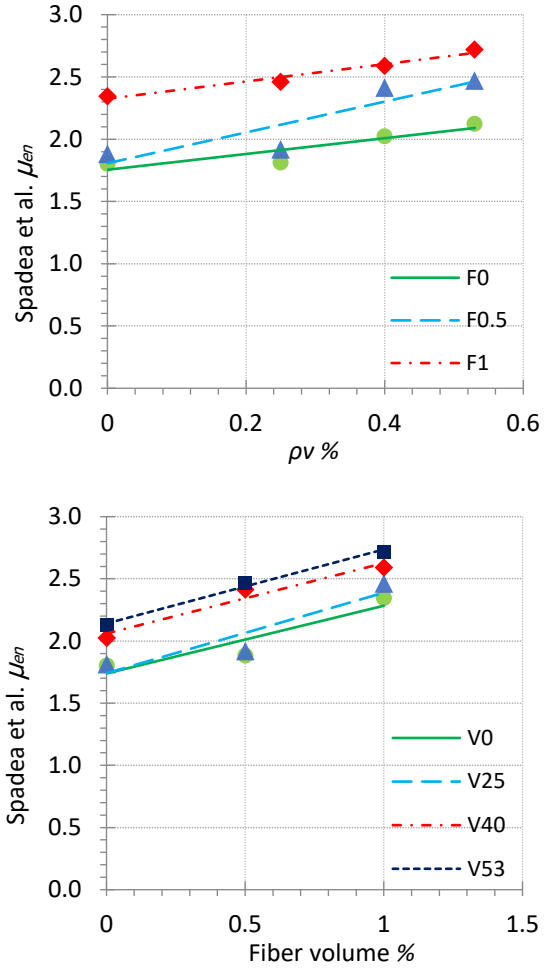

Figure 10. Parameters' effect on ductility index by Spadea et al.'s proposition.

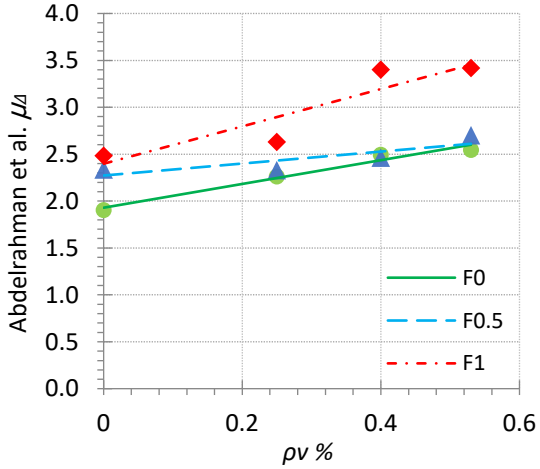

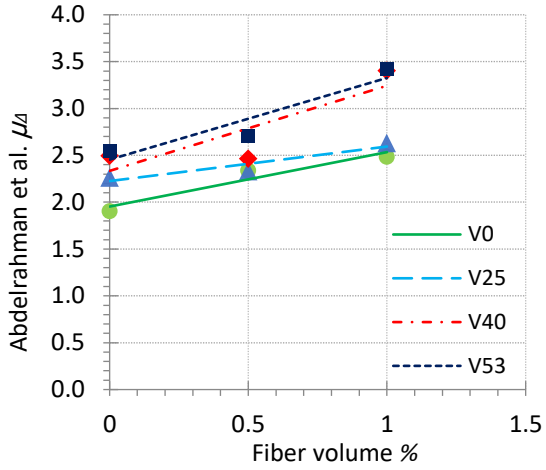

Figure 11. Parameters' effect on ductility index by Abdelrahman et al.'s proposition.

3.8.2 Concrete Strength Capacity V_c and STM of CSA S806-12 [22]

The Canadian code CSA S806-12 [22] considers the arch action effect on member shear strength by the coefficient factor ka, and also takes into account the size effect by the coefficient factor k_s, A coefficient that considers the effect of the moment at the section k_m and a coefficient that considers the effect of reinforcement rigidity on its shear strength k_r.

$$V_c = 0.05\lambda k_m k_r k_a k_s (f_c')^{1/3} b_w d_v \quad (7)$$

$$k_m = \sqrt{d/a} \leq 1.0 \quad (8)$$

$$k_r = 1 + \left(E_f \rho_f\right)^{1/3} \quad (9)$$

$$1.0 \leq k_a = 2.5/(d/a) \leq 2.5 \quad (10)$$

$$k_s = 750/(450 + d) \leq 1.0 \quad (11)$$

$$0.11\sqrt{f_c'} b_w d_v \leq V_c \leq 0.22\sqrt{f_c'} b_w d_v \quad (12)$$

Where λ is the concrete density account factor, d effective depth, dv effective shear depth.

The Canadian code CSA S806-12 recommends STM for FRP-reinforced members, whereas CSA A23.3-19 recommends STM for steel-reinforced members.

Struts compressive strength F_{ns}:

$$F_{ns} = \phi_c f_{cu} A_{cs} \quad (13)$$

$$f_{cu} = \frac{f_c'}{0.8+170\varepsilon_1} \quad (14)$$

$$\varepsilon_1 = \varepsilon_f + \left(\varepsilon_f + 0.002\right) cot^2\theta_s \quad (15)$$

Tie tensile strength F_{nt}:

$$F_{nt} = 0.65\phi_F f_{Fu} A_{FT} \quad (16)$$

Nodal zone compressive F_{nn}:

$$F_{nn} = \phi_c \beta_n f_c' A_{nz} \quad (17)$$

$$\beta_n = \begin{cases} 0.85\ for\ nodal\ zone\ bounded\ by\ bearing\ area\ and\ strut \\ 0.75\ for\ nodal\ zone\ anchoring\ one\ tie \\ 0.65\ for\ nodal\ regions\ anchoring\ more\ than\ one\ ties \end{cases} \quad (18)$$

Where $\emptyset_c$ is a resistance factor for concrete, A_{cs} is the cross-sectional area of the concrete strut, ε_f is the tensile strain in the tie bar, θs is the smallest angle that can be made between a strut and its adjacent ties, $\emptyset_F$ is the FRP reinforcement's resistance factor, f_{Fu} ultimate strength of FRP reinforcement, A_{FT} is the longitudinal FRP reinforcement area in the tension tie, A_{nz} is the nodal zone face area.

3.8.3 Shear Concrete Capacity V_c by Zhang et al. [23]

Zhang et al. [23] derived a generic closed-form solution from a segmental approach to mechanics for the shear capacity quantification of RC beams without stirrups, regardless of reinforcement or concrete type. $V_c = \frac{0.345 b_w n\rho d\left(\sqrt{1+\frac{2}{n\rho}}-1\right) f_c'^{\,0.665}}{1-\frac{Dd}{d-0.333 n\rho d\left(\sqrt{1+\frac{2}{n\rho}}-1\right)}}$

$$for\ a/d\ <\ 3.14 \quad (19)$$

$$n = \frac{E_f}{E_c} \quad (20)$$

$$D = -0.195\left(\frac{a}{d}\right)^2 + 0.511\left(\frac{a}{d}\right) + 0.212 \quad (21)$$

3.8.4 Shear Capacity Vn by Nehdi et al. [24]

Nehdi et al. [24] propose a simple yet improved formula, based on a genetic algorithm technique, to determine the shear capacity of a concrete deep beam reinforced with FRP. Nehdi et al. [24] calculated only the contribution of vertical web reinforcement.

$$V_n = V_{cf} + V_{fv} \quad (22) V_{cf} = 2.1\left(\frac{f_c'\,\rho_{fl} d}{a}\frac{E_{fl}}{E_s}\right)^{0.3} b_w d \times 2.5\frac{d}{a}$$

$$for\ a/d\ <\ 2.5 \quad (23)$$

$$V_{fv} = 0.5\left(\rho_{fv} f_{fv}\right)^{0.5} \quad (24)$$

Where V_{cf} is the shear capacity of a concrete beam reinforced with FRP without web reinforcement, V_{fv} is the FRP stirrups' shear capacity, ρ_{fl} is the longitudinal reinforcement ratio, E_{fl} The modulus of elasticity of the FRP bar is E_s is the modulus of elasticity of steel, ρ_{fv} is the shear reinforcement ratio, f_{fv} ultimate capacity of shear reinforcement.

The performance of the previous shear capacity prediction methods for the specimens included in the current study and the test result of the shear capacity of specimens as listed in Table 8.

Table 8. The test result and other methods of prediction.

Specimen	*Test* V_{max} kN	ACI 440-22 V_c kN	V_{exp}/V_c ACI 440-22 V_c	CSA S806-12 STM V_n kN	V_{exp}/V_n CSA S806 STM	CSA S806-12 V_c kN	V_{exp}/V_c CSA S806	Zhang et al. V_c kN	V_{exp}/V_c Zhang et al.	Nehdi et al. V_n kN	V_{exp}/V_n Nehdi et al.
F0V0	279.1	24.6	11.3	205	1.36	175.2	1.59	106	2.63	134.2	2.08
F0V25	286.1	*			1.40	*		*	*	290.53	0.98
F0V40	291.5	*			1.42	*		*	*	331.95	0.88
F0V53	301	*			1.47	*		*	*	361.82	0.83
F0.5V0	290	26.5	11	241	1.21	185	1.57	117	2.48	140.8	2.06
F0.5V25	302.6	*			1.26	*		*	*	297.14	1.02
F0.5V40	312.1	*			1.30	*		*	*	338.55	0.92
F0.5V53	324.5	*			1.35	*		*	*	368.42	0.88
F1V0	304.6	27.2	11.2	262	1.16	190	1.60	122	2.50	144.5	2.11
F1V25	310.8	*			1.19	*		*	*	300.81	1.03
F1V40	328.2	*			1.25	*		*	*	342.22	0.96
F1V53	351.6	*			1.34	*		*	*	372.10	0.94
Mean			11.16		1.31		1.59		2.54		1.22
S.D			0.19		0.1		0.02		0.08		0.52
COV			1.71		7.46		1.06		3.26		42.47

* The method does not include web reinforcement in the calculation of shear capacity

The CSA S806-12 STM [22] and Nehdi et al. [24] are the best methods to predict the shear capacity of FRP deep beams. It can be noted that the other methods are conservative. The method of Nehdi et al. [24] for predicting shear capacity is quite reasonable for a beam with vertical web reinforcement. Still, it is overly conservative for a beam with no web reinforcement and does not account for horizontal web reinforcement. The effect of steel fiber is not directly included; it is accounted for in the concrete compressive strength.

4. Conclusions

Twelve supported deep beams were tested to failure. From the test results, it can be concluded that the vertical web reinforcement affects the failure load and mid-span deflection. The test results analysis shows that the increase of vertical web reinforcement ratio from (0 to 0.0053) increases the failure load and decreases mid-span deflection for the same fiber volume fraction.

The addition of steel fiber volume fraction (1%) increases the failure load up to 16.8% and decreases mid-span deflection 24.29% for the same vertical web reinforcement.

The ratio of PF)cr /Pmax increases significantly with increasing steel fiber content, more than with increasing web reinforcement ratio, due to the significant effect of steel fibers on the tensile strength of concrete. The diagonal crack load percentage at maximum load increases with increasing fiber volume fraction and vertical web reinforcement ratio.

The CSA S806-12 STM and Nehdi et al. are the best methods to predict the shear capacity of FRP deep beam, while ACI 440 and CSA S806 are conservative. Zhang et al. do not include the contribution of web reinforcement. The method for shear capacity calculation is inaccurate in predicting the shear capacity of a fibrous FRP-reinforced deep beam.

The most important feature of cracks in beams with fiber volume fraction is that they are not sharp, because the two crack faces are bridged by fibers and resist tensile forces, thereby increasing the load capacity to failure.

Acknowledgements

The author is grateful to the civil engineering department and the staff of the structural and construction materials laboratories for the facilities provided during the preparation of the experimental part of the present research work. Also, the author would like to express his appreciation to the staff of the Journal of Engineering and Sustainable Development.

Conflict of Interest

The authors declare that there are no conflicts of interest regarding the publication of this manuscript.

Author Contribution Statement

Eklas Hatto Hashim conducted the experimental part, prepared the research, and performed the required computations.
Hassan Falah Hassan proposed the research problem.
Both authors supervised the work, discussed the results, and contributed to the final manuscript.

References

[1] ACI Committee 318, "Building code requirements for structural concrete (ACI 318-19) and commentary," American Concrete Institute, Farmington Hills, MI, USA, 2019.

[2] CSA, "CSA A23.3-19: Design of concrete structures," Canadian Standards Association, Ottawa, ON, Canada, 2019.

[3] D. Darwin, C. W. Dolan, and A. H. Nilson, Design of Concrete Structures, 15th ed. New York, NY, USA: McGraw-Hill Education, 2016.

[4] ACI Committee 440, "Guide for the design and construction of structural concrete reinforced with FRP bars (ACI 440.11-22)," American Concrete Institute, Farmington Hills, MI, USA, 2022.

[5] M. Said, M. A. Adam, and A. S. Shanour, "Experimental and analytical shear evaluation of concrete beams reinforced with glass fiber reinforced polymer bars," Construction and Building Materials, vol. 102, pp. 574–591, 2016. doi: https://doi.org/10.1016/j.conbuildmat.2015.10.185.

[6] K. Mohamed, A. S. Farghaly, and B. Benmokrane, "Effect of vertical and horizontal web reinforcement on the strength and deformation of concrete deep beams reinforced with GFRP bars," Journal of Structural Engineering, vol. 143, no. 8, p. 04017079, 2017. doi: https://doi.org/10.1061/(ASCE)ST.1943-541X.0001786.

[7] M. K. Nassif, A. M. Erfan, O. T. Fadel, and T. A. El-Sayed, "Flexural behavior of high strength concrete deep beams reinforced with GFRP bars," Case Studies in Construction Materials, vol. 15, p. e00613, 2021. doi: https://doi.org/10.1016/j.cscm.2021.e00613.

[8] H. Chen, W. J. Yi, Z. J. Ma, and H. J. Hwang, "Modeling of shear mechanisms and strength of concrete deep beams reinforced with FRP bars," Composite Structures, vol. 234, p. 111715, 2020. doi: https://doi.org/10.1016/j.compstruct.2019.111715.

[9] M. Kazemi, M. Daneshfar, Y. Zandi, S. A. Agdas, N. Yousefieh, L. Mohammadifar, and J. Li, "Effects of the concrete strength and FRP reinforcement type on the non-linear behavior of concrete deep beams," Sustainability, vol. 14, no. 7, p. 4136, 2022. doi: https://doi.org/10.3390/su14074136.

[10] P. Swaminathan and G. Kumaran, "Theoretical and experimental study on the behaviour of deep beams reinforced internally using hybrid fibre-reinforced polymer rebars with and without web openings," in Advances in Construction Materials and Structures: Select Proceedings of ICON 2019, Singapore: Springer, pp. 141–154, 2021. doi: https://doi.org/10.1007/978-981-15-9162-4_12.

[11] F. Abed, M. K. Sabbagh, and A. S. Karzad, "Effect of basalt microfibers on the shear response of short concrete beams reinforced with BFRP bars," Composite Structures, vol. 269, p. 114029, 2021. doi: https://doi.org/10.1016/j.compstruct.2021.114029.

[12] S. A. Hosseini, M. Nematzadeh, and C. Chastre, "Prediction of shear behavior of steel fiber-reinforced rubberized concrete beams reinforced with glass fiber-reinforced polymer (GFRP) bars," Composite Structures, vol. 256, p. 113010, 2021. doi: https://doi.org/10.1016/j.compstruct.2020.113010.

[13] Y. G. Abtan and H. F. Hassan, "A review of behavior of reinforced concrete deep beams," Journal of Engineering and Sustainable Development, vol. 24, no. 5, pp. 66–77, 2020. doi: https://doi.org/10.31272/jeasd.24.5.10.

[14] A. Bediwy, K. Mahmoud, and E. El-Salakawy, "Structural behavior of FRCC layered deep beams reinforced with GFRP headed-end bars," Engineering Structures, vol. 243, p. 112648, 2021. doi: https://doi.org/10.1016/j.engstruct.2021.112648.

[15] ACI Committee 440, "ACI 440.1R-15: Guide for the design and construction of structural concrete reinforced with FRP bars," American Concrete Institute, Farmington Hills, MI, USA, 2015.

[16] M. A. El Zareef and M. E. El Madawy, "Effect of glass-fiber rods on the ductile behaviour of reinforced concrete beams," Alexandria Engineering Journal, vol. 57, no. 4, pp. 4071–4079, 2018. doi: https://doi.org/10.1016/j.aej.2018.03.012.

[17] L. G. Jaeger, A. A. Mufti, and G. Tadros, "The concept of the overall performance factor in rectangular-section reinforced concrete beams," in Proceedings of the Third International Symposium on Non-Metallic (FRP) Reinforcement for Concrete Structures (FRPRCS-3), vol. 2, Japan Concrete Institute, Sapporo, Japan, Oct. 1997, pp. 551–558.

[18] G. Spadea, F. Bencardino, and R. N. Swamy, "Strengthening and upgrading structures with bonded CFRP sheets: Design aspects for structural integrity," in Proceedings of the Third International Symposium on Non-Metallic (FRP) Reinforcement for Concrete Structures (FRPRCS-

3), vol. 1, Japan Concrete Institute, Sapporo, Japan, Oct. 1997, pp. 629–636.

[19] A. A. Abdelrahman, G. Tadros, and S. H. Rizkalla, "Test model for the first Canadian smart highway bridge," ACI Structural Journal, vol. 92, no. 4, pp. 451–458, 1995.

[20] Canadian Commission on Building and Fire Codes, National Building Code of Canada 2020, vol. 1. Ottawa, ON, Canada: National Research Council Canada, 2020.

[21] J. Thomas and S. Ramadass, "Improved empirical model for the strut efficiency factor and the stiffness degradation coefficient for the strength and the deflection prediction of FRP RC deep beams," Structures, vol. 29, pp. 2044–2066, 2021. doi: https://doi.org/10.1016/j.istruc.2020.12.039.

[22] CSA, "CSA S806-12: Design and construction of building components with fiber-reinforced polymers," Canadian Standards Association, Mississauga, ON, Canada, 2012.

[23] T. Zhang, D. J. Oehlers, and P. Visintin, "Shear strength of FRP RC beams and one-way slabs without stirrups," Journal of Composites for Construction, vol. 18, no. 5, p. 04014007, 2014. doi: https://doi.org/10.1061/(ASCE)CC.1943-5614.0000469.

[24] M. Nehdi, H. El Chabib, and A. A. Saïd, "Proposed shear design equations for FRP-reinforced concrete beams based on genetic algorithms approach," Journal of Materials in Civil Engineering, vol. 19, no. 12, pp. 1033–1042, 2007. doi: https://doi.org/10.1061/(ASCE)0899-1561(2007)19:12(1033).